

## HYDRODYNAMIC TRANSIENT ASSESSMENT OF A DRAINING TANK

Ludmila M. Rechiman<sup>a,b</sup>, Mariano I. Cantero<sup>a,b,c</sup> and Enzo A. Dari<sup>a,b,c</sup>

<sup>a</sup>*Departamento de Mecánica Computacional CNEA. Centro Atómico Bariloche R8402AGP, Río Negro, Argentina.*

<sup>b</sup>*Instituto Balseiro, UNCu-CNEA, Argentina.*

<sup>c</sup>*Investigator member of CONICET, Argentina.*

**Keywords:** Free Surface simulation, CFD, OpenFOAM.

**Abstract.** In this paper we present a simplified model using OpenFOAM® suite to study the hydrodynamic behavior of a draining tank, which is part of a second shut down system of an experimental nuclear reactor. This problem involves the presence of a free surface between a liquid and a cover gas which should be accurately described during the draining transient of the liquid inside the tank. By using a three grid approach for the relevant parameter to compute the height of drained liquid, we bound the uncertainty in the calculations induced by the spatial discretization in agreement with the achievable computing times. We compute the level of the surface in a local manner and by using global balances. We compare the solution for the discharge dynamics obtained by the two different methods showing consistency and concordance between them. We also present an analytical approach which points out the lowest threshold for the discharge time.

## 1 INTRODUCTION

A nuclear reactor together with the space shuttle are maybe the two more complex machines made by man due to each one is composed by a large amount of diverse interacting systems. Many of these systems involve fluid flow, heat transfer, chemical and nuclear reactions among the main ones.

In this work we focus on develop a simple model of a system composed mainly by a draining tank which is part of a second shut down system of an experimental nuclear reactor. The primary function of this safety system is to shut down the reactor by removing the neutronic liquid reflector inside of it through draining just due to the action of gravity. This system requires a mesoscale description to analyze the fluid dynamics inside the tank while is draining.

The description of fluid flow systems can be made from two complementary points of view: experimental approach and numerical approach. One of the principal interests of using numerical simulations to study fluids in movement is that the costs involved are lower than an experimental approach allowing parametric studies which are important in a design stage. This is true if the problem to analyze involves a real scale geometry one to one.

Many times the systems to analyze in the nuclear industry are large enough that are modeled as networks of control volumes composed by 1-D elements connected by flow junctions (NEA (2007), Hilal (2012)). These concepts are implemented in thermohydraulic codes such as RELAP, TRACE, CATHARE and ATHLET which allows to obtain a macroscopic description of the problem.

On the other hand, a mesoscale description of the problem could be obtained by using numerical tools usually known as CFD codes. The incorporation of CFD approach as a well-established methodology is rising due to the monotonic growth of the available computing power in the last thirty years which allows simulations of increasing complexity involving larger geometries as well as getting better time and space resolution of the computed solutions (EPRI (2014), IAEA-TECDOC-1379 (2003)).

Due to the size of typical problems present in the nuclear industry, these two descriptions become complementary in the sense that in order to fully describe complex systems they can be linked. The last means that a localized 3-D computation should be performed where it is required but in the framework of an overall macroscale description, which usually impose values for the boundary conditions of the three-dimensional model (NEA (2007)).

In order to get a model to describe the three dimensional fluid dynamics of a draining tank we use the OpenFoam framework (OpenFOAM® (2014)) developed by Jasak (1996). High quality CFD analysis has many steps that requires a fussy methodology. In first place a suitable discretization of the geometric domain, some times a parallelization technique to optimize the computing times, solving the right equations that model the problem, the visualization of the results and a verification and validation process.

As a test of concept, this work tries to go through all the needed steps to solve the CFD problem taking knowledge and handle the main details involved to achieve the required engineering solution.

The paper is organized as follows: in Sec.(2) we describe the principal features of the problem and we present a theoretical solution. In Sec.(3) we describe the numerical model used in the simulations. In Sec.(4) we present the discretization of the geometric domain used for computing the numerical solution and we detail the boundary conditions used along the work. In Sec.(5) we present and discuss our results with special attention to uncertainty report. Finally in Sec.(6) we summarize our conclusions.

## 2 DESCRIPTION OF THE PROBLEM AND THEORETICAL APPROACH

In the present work, we consider a tank of cylindrical shape with height  $H = 1.2m$  and radius  $R = 1.0m$ . At the bottom of the tank there is an orifice of radius  $R_0 = 0.12m$ . The tank is open on top, and the reference pressure is equal above and below it. The tank is initially filled with light water up to  $h = 1.0m$ . Figure (1) shows the basic configuration.

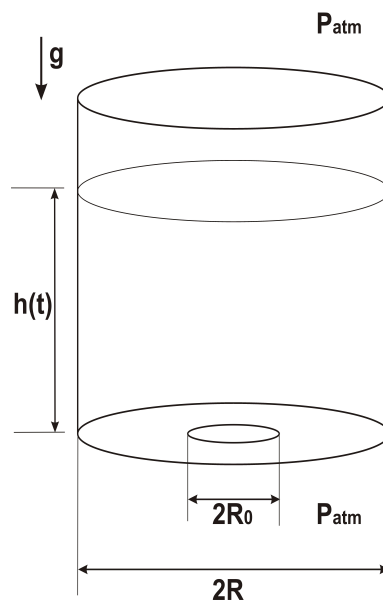


Figure 1: Schematic diagram of the problem.

An analytical approach can be made by applying the conservation of mechanical energy (Bird et al. (2002)). From first principles, the draining time of the liquid due to the action of the volumetric gravity force in the geometry described by Figure (1) can be obtained by solving:

$$2h(t)\frac{d^2h(t)}{dt^2} - \left[\frac{R^4}{R_0^4} - 1\right]\left(\frac{dh(t)}{dt}\right)^2 + 2gh(t) = 0 \quad (1)$$

This second order non-linear ODE allows us to obtain the dependence of the liquid height within the tank with time. We conveniently define:

$$N = \frac{R^4}{R_0^4}$$

$$\eta = \frac{h}{h_0}$$

The initial conditions (IC) for the Eq.(1) are:

$$\text{IC 1) } t = 0 \rightarrow h = h_0$$

$$\text{IC 2) } t = 0 \rightarrow \frac{dh}{dt} = 0$$

The final draining time of the whole liquid in the tank expressed in a compact manner is:

$$t_{drained} = -\sqrt{\frac{(N-2)h_0}{2g}} \int_0^1 \frac{d\eta}{\sqrt{\eta - \frac{2\eta^{(N-1)}}{N}}} \quad (2)$$

Equation (2) can be solved by applying an adaptive Gauss-Kronrod quadrature integrator. The results are displayed in Figure (2). It can be seen that a monotonic and smooth evolution of the liquid height is obtained. The height of the remaining liquid inside the tank at the particular time  $t = 15s$  is  $h = 0.27m$ , and by that instant the volumetric flow is nearly half than the initial one.

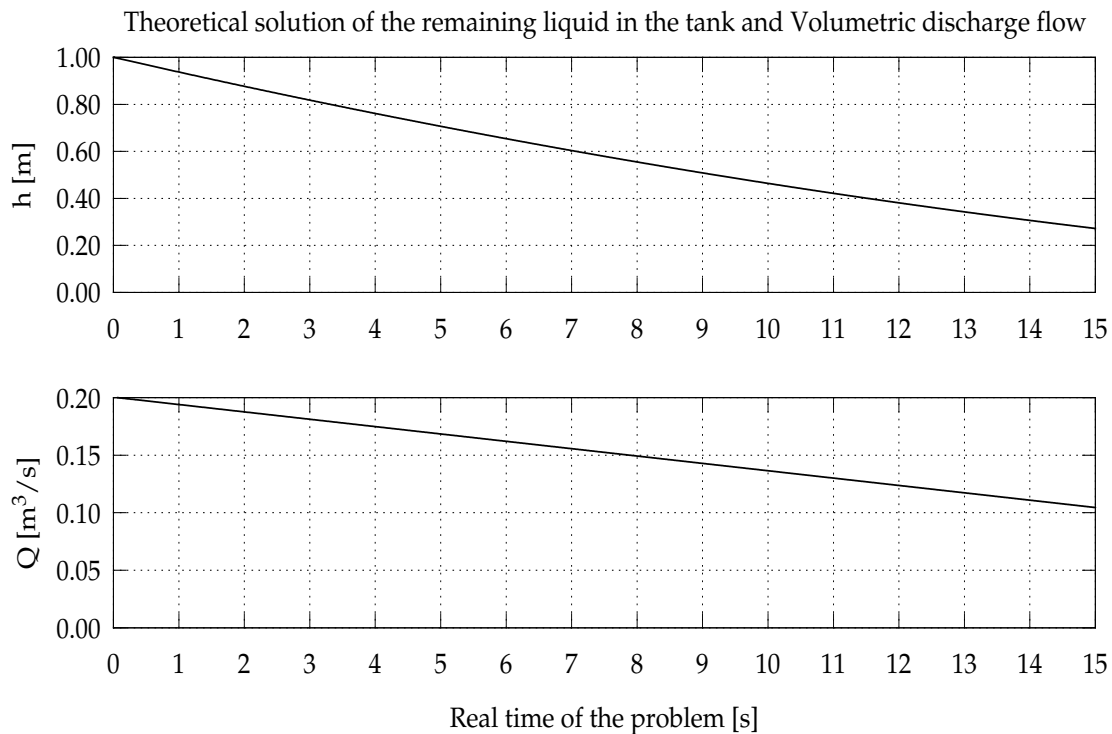


Figure 2: (Upper panel) Temporal evolution of the theoretical solution for the liquid height in the cylindrical tank. The parameters for the problem are:  $R = 1.00m$ ,  $R_0 = 0.12m$ ,  $h_0 = 1.0m$ ,  $g = 9.81 \frac{m}{s^2}$ . (Lower panel) Volumetric discharge flow.

### 3 NUMERICAL MODEL

We also solved the problem using OpenFOAM® to study the hydrodynamic behavior of the cylindrical draining tank in three dimensions.

The **interFoam** precompiled solver for the **Unsteady Reynolds Averaged Navier Stokes Equations** (URANSE) was employed (UG.OpenFoam.ESI (2013)). In this work, turbulence closure was done by using the two-equation model  $\kappa - \varepsilon$  (Durbin and Pettersson-Reif (2011)). The solver also includes the surface tension effect between the phases, and the description of the interphase is made by Volume of Fluid method (Hirt and Nichols (1981)). In this method, a function  $\alpha$  indicates the relative fraction of gas and liquid in each cell of the physical domain. The function  $\alpha$  is transported with the mean velocity of the fluid ( $\bar{\mathbf{U}}$ ). It should be emphasized that with the present model we solve the mean velocity of the fluid and we do not describe the instantaneous flow velocity ( $\mathbf{U}$ ) with all the spatial and temporal details.

It is also important to notice that in this model an effective fluid is taken into account along the whole domain, which changes its properties according to the indicator function  $\alpha$  in each cell in the following form:

$$\rho = \alpha\rho_L + (1 - \alpha)\rho_G$$

$$\mu = \alpha\mu_L + (1 - \alpha)\mu_G$$

$$\bar{\mathbf{U}} = \alpha\bar{\mathbf{U}}_L + (1 - \alpha)\bar{\mathbf{U}}_G$$

The subscripts **G** and **L** denote the *gas* and *liquid* phases respectively,  $\rho$  is the density and  $\mu$  is the dynamic viscosity of the fluid.

In the present problem we considered an isothermal fluid system composed by two initially segregated, incompressible and newtonian phases (light water and air). The system of equations which describes the problem is:

$$\left\{ \begin{array}{l} \frac{\partial \rho}{\partial t} + \nabla \cdot (\rho \bar{\mathbf{U}}) = 0 \quad \text{Incomp.} \Rightarrow \frac{\partial \bar{U}_i}{\partial x_i} = 0 \quad i = x, y, z \\ \frac{\partial \bar{U}_i}{\partial t} + \bar{U}_j \frac{\partial \bar{U}_i}{\partial x_j} = -\frac{1}{\rho} \frac{\partial \bar{p}}{\partial x_i} + \frac{\partial}{\partial x_j} (\nu \frac{\partial \bar{U}_i}{\partial x_j} - \overline{U'_i U'_j}) + f_i + \sigma \xi \nabla \alpha \\ \frac{\partial \kappa}{\partial t} + \bar{U}_j \frac{\partial \kappa}{\partial x_j} = -\overline{U'_i U'_j} \frac{\partial \bar{U}_i}{\partial x_j} - \varepsilon + \frac{\partial}{\partial x_j} [(\nu + \nu_T) \frac{\partial \kappa}{\partial x_j}] \\ \frac{\partial \varepsilon}{\partial t} + \bar{U}_j \frac{\partial \varepsilon}{\partial x_j} = -C_{1\varepsilon} \frac{\varepsilon}{\kappa} \overline{U'_i U'_j} \frac{\partial \bar{U}_i}{\partial x_j} - C_{2\varepsilon} \frac{\varepsilon^2}{\kappa} + \frac{\partial}{\partial x_j} [(\nu + \frac{\nu_T}{\gamma_0}) \frac{\partial \varepsilon}{\partial x_j}] \\ \frac{\partial \alpha}{\partial t} + \nabla \cdot (\alpha \bar{\mathbf{U}}) + \nabla \cdot (\alpha(1 - \alpha)(\bar{\mathbf{U}}_L - \bar{\mathbf{U}}_G)) = 0 \\ \xi = -\nabla \cdot (\frac{\nabla \alpha}{|\nabla \alpha|}) \end{array} \right. \quad (3)$$

Here  $\nu_T$  is the turbulent kinematic viscosity which is the coupling variable between the URANSE and the  $\kappa - \varepsilon$  model,  $\nu$  is the kinematic viscosity,  $\sigma$  is the surface tension,  $\xi$  is the curvature of the free surface,  $\kappa$  is the turbulent kinematic energy,  $\varepsilon$  is the dissipation rate of the turbulent kinematic energy, and  $C_{1\varepsilon}$ ,  $C_{2\varepsilon}$  and  $\gamma_0$  are characteristic constants of the  $\kappa - \varepsilon$  model:  $C_{1\varepsilon} = 1.44$ ,  $C_{2\varepsilon} = 1.92$ ,  $\gamma_0 = 1.30$ , and  $C_\mu = 0.09$ .

The coupling between the equation for  $\kappa$  and the equation for  $\varepsilon$  with the momentum equation is made by the turbulent kinematic viscosity.

$$\nu_T = C_\mu \frac{\kappa^2}{\varepsilon}$$

The Reynolds stress term  $\overline{U'_i U'_j}$  is given by:

$$-\overline{U'_i U'_j} = \nu_T \left( \frac{\partial \bar{U}_i}{\partial x_j} + \frac{\partial \bar{U}_j}{\partial x_i} \right) - \frac{2}{3} \kappa \delta_{ij}$$

The system employs the  $p_{rgh}$ , which is the difference between the real pressure field  $p$  and the field  $\rho \vec{\mathbf{g}} \cdot \vec{\mathbf{x}}$ :

$$p_{rgh} = p - \rho \vec{\mathbf{g}} \cdot \vec{\mathbf{x}}$$

Here  $\vec{\mathbf{g}}$  is the gravity acceleration and  $\vec{\mathbf{x}}$  is the location of the fluid particle.

The transient solutions were obtained with the PIMPLE algorithm in the PISO mode. The numerical method applied to solve each differential operator of the system of equations Eq.(3) and the order of convergence are listed in Table (1). In the OpenFOAM framework the specification of how each differential operator will be solved is made through the dictionary *fvSchemes*. Table (1) shows the scheme employed to solve each operator in the system of equations given by Eq.(3). The *Gaussian scheme* refers to the *Standard Gaussian finite volume integration* that is based on summing values on cell faces which must be interpolated from cell centers (SG.OpenFoam.ESI (2013),UG.OpenFoam.ESI (2013)). The *interpolationSchemes* sub-dictionary allows the user to specify the interpolation method for the task of calculating the value of the analyzed variable on the corresponding cell face based on the known values at cell centers.

Term	Scheme	Order of convergence	Interpolation scheme
$\frac{\partial}{\partial t}, \frac{\partial^2}{\partial t^2}$	Euler	$O(h)$	
$\nabla$	Gauss	$O(h^2)$	linear
$\nabla \cdot (\rho\phi, U)$	Gauss	$O(h^2)$	linear
$\nabla \cdot (\phi, \alpha)$	Gauss	$O(h^2)$	vanLeer
$\nabla \cdot (\phi, \kappa)$	Gauss	$O(h)$	upwind
$\nabla \cdot (\phi, \varepsilon)$	Gauss	$O(h)$	upwind
$\nabla^2$	Gauss	$O(h^2)$	linear corrected

Table 1: Numerical scheme and order of convergence of each differential operator of the system of Eq.(3).

#### 4 MESH GENERATION AND BOUNDARY CONDITIONS

The meshes used in this problem were generated using Gmsh Version 2.4.2 (Geuzaine et al. (2009a),Geuzaine et al. (2009b)). Gmsh is an open-source three-dimensional finite element grid generator. In Figure (3) we display the geometric domain which is a cylinder of 1.2m height and 1.0m of radius. At the bottom of the cylinder, there is an orifice with diameter 0.24m, which may be centered in some cases and non-centered in others. The meshes are non-structured composed by tetrahedrons, in which no transformation exists that could get a meeting of the grid lines at right angles, and besides the nodes coordinates, a connectivity list should be specified (Dari and Buscaglia (1994)). Due to the fact that in a next step it is planned to add more details inside the tank, we choose a non-structured mesh because of the ability of nodalize very complex geometries. In Figure (4) we show a typical surface mesh used along this work. During the meshing procedure, *physical surfaces* should be defined in order to apply the associated boundary conditions for each one. For this problem we have defined four *physical surfaces* that bounds the geometric domain:

- Upper wall
- Floor
- Lateral wall
- Hole

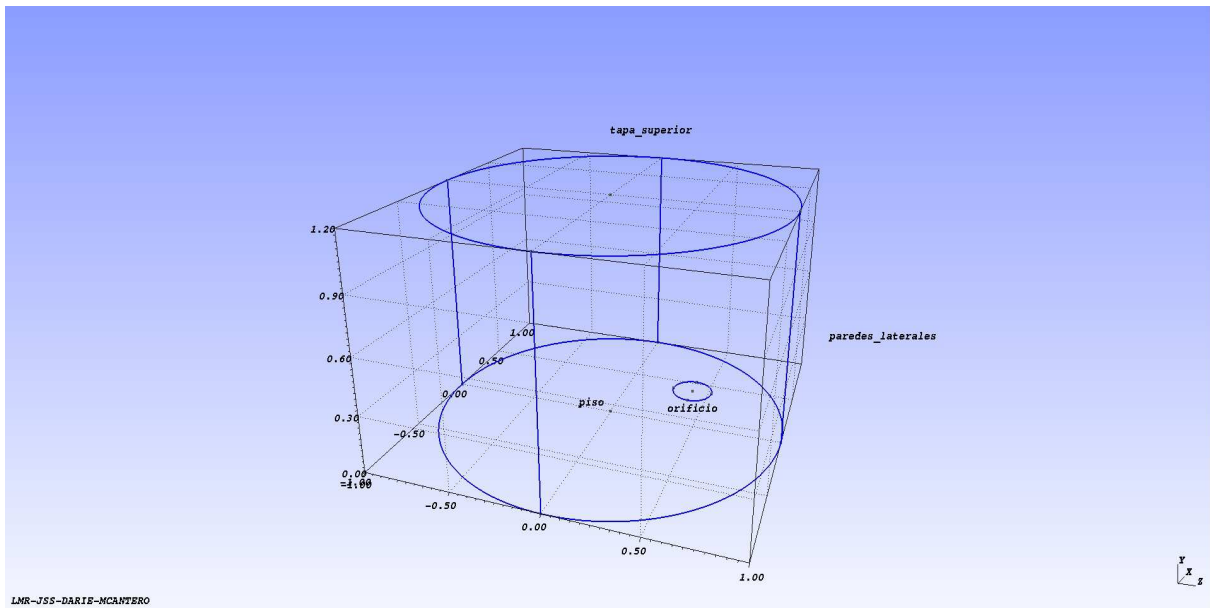


Figure 3: Geometric domain. Definition of “Physical Groups” where BC will be applied.

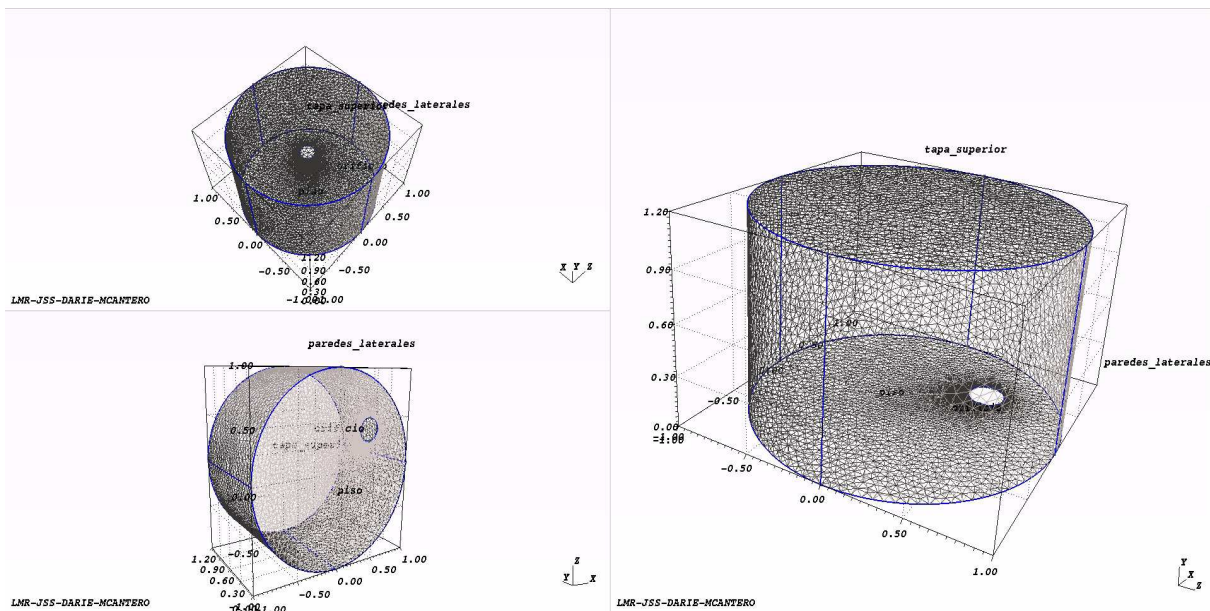


Figure 4: Non-structured mesh of 703707 tetrahedrons. Only the surface mesh is shown.

Mesh number	N tetrahedrons	Volume [m <sup>3</sup> ]	$h_{cell}$ [m]	Aspect ratio	Min. Vol. [m <sup>3</sup> ]	Max. Vol. [m <sup>3</sup> ]	Mesh non-orth Max. angle [°]	Max. Skewness
1	2260711	3.76970	0.01186	9.0000	$1.97 \times 10^{-10}$	$1.66 \times 10^{-5}$	70.5288	1.0000
2	727575	3.76942	0.01730	7.6197	$1.26 \times 10^{-9}$	$4.18 \times 10^{-5}$	70.5295	0.9985
3	370512	3.76912	0.02167	7.8162	$4.83 \times 10^{-9}$	$8.67 \times 10^{-5}$	71.1327	0.8934

Table 2: Main properties of meshes.

Near the discharge hole, a graded refinement was applied (Figure (4)). Table(2) describes the main features of the meshes used in this work. Mesh number (1) is the finest one and the results obtained with it will be used as the “true solution”.

There are some mesh features regarding grid quality that may affect the accuracy of the solution obtained by the finite volume method (Ferziger and Perić (2002)). In first place, the calculation

of convective fluxes have maximum accuracy if the line connecting the two centers of neighboring control volumes (CV) pass through the center of the common face. A measure of the distance between the center of the face and the intersection of the line connecting the two CV centers with the common face relative to the size of the cell face is known as *skewness*. The smaller the skewness is, better quality of the mesh is get. Skewness can be reduced through local grid refinement. It can be seen from Table (2) that mesh (3) has the highest skewness.

On the other hand, a maximum accuracy in the computation of diffusive flux is obtained when the line connecting the neighboring CV centers is orthogonal to the cell face and passes through the cell-face center. This is due to the fact that orthogonality increases the accuracy of the calculation of the derivative in the direction normal to the cell-face. Another parameter important for accuracy is the angle between the line connecting neighboring CV centers and the cell-face normal (Mesh non-orth Max.angle). In Table (2) it can be seen that the three meshes have almost the same *non-orth Max. angle*. The *aspect ratio* is another parameter which express the ratio between the longest and the shortest edges. It should be as close as unity as possible due to the fact that tetrahedrons with large aspect ratios may induce oscillations in the calculation of velocity component in the direction of the longest side of the CV. Further details can be check in [Ferziger and Perić \(2002\)](#).

The boundary conditions (BC) applied on each *physical surface* are listed in Table (3).

Physical surface	BC U	BC $p_{rgh}$	BC $\nu_T$	BC $\kappa$	BC $\varepsilon$	BC $\alpha$
Upper wall	pressureInletOutletVelocity	totalPressure	calculated	inletOutlet	inletOutlet	inletOutlet
Floor	slip	buoyantPressure	nutkWallFunction	kqRWallFunction	epsilonWallFunction	zeroGradient
Lateral wall	slip	buoyantPressure	nutkWallFunction	kqRWallFunction	epsilonWallFunction	zeroGradient
Hole	zeroGradient	fixedValue	calculated	zeroGradient	zeroGradient	zeroGradient

Table 3: Boundary condition applied on each *physical surface*.

## 5 RESULTS

A three grid approach was used in order to quantify the uncertainty in the calculations due to the spatial discretization. To make the analysis we have chosen the modulus of the velocity averaged in the discharge hole area, because it is the variable employed to make the calculation of the remaining liquid height in the tank by using the mass conservation. The Table (4) sum up the values for  $|U|$  for the first second of time evolution of the problem. To quantify the discrepancy between them, the Table (5) shows the relative error assuming that the most precise solution is obtained with the mesh (1). It can be seen that for the mesh (2), an error lower than 0.050% is achieved and the computing time is much lower than using the mesh (1). For the following simulations, meshes of sizes similar to mesh (2) were used, and the domain decomposition based on the graph partitioning method implemented through Scotch library was used in order to optimize the computing times ([Pellegrini \(2009\)](#)). It should be remarked that all these calculations were made considering a centered discharge hole.

In Figure (5) we show the velocity profile in the direction of the principal component of the flow along the discharge hole computed with the three meshes described in Table (4). It can be seen that a quite good agreement exists between the solution obtained with mesh (2) and the finest mesh number (1). In this case the relative error is lower than <2% far from edges but suddenly grows toward the hole boundaries. It can also be seen that the solution obtained with the coarsest mesh number (3) reveal that a velocity profile with lower mean velocity than the case associated with mesh (1) and (2) is computed. For further analysis, meshes with similar characteristics than mesh (2) will be used as a compromise solution with the computing time.

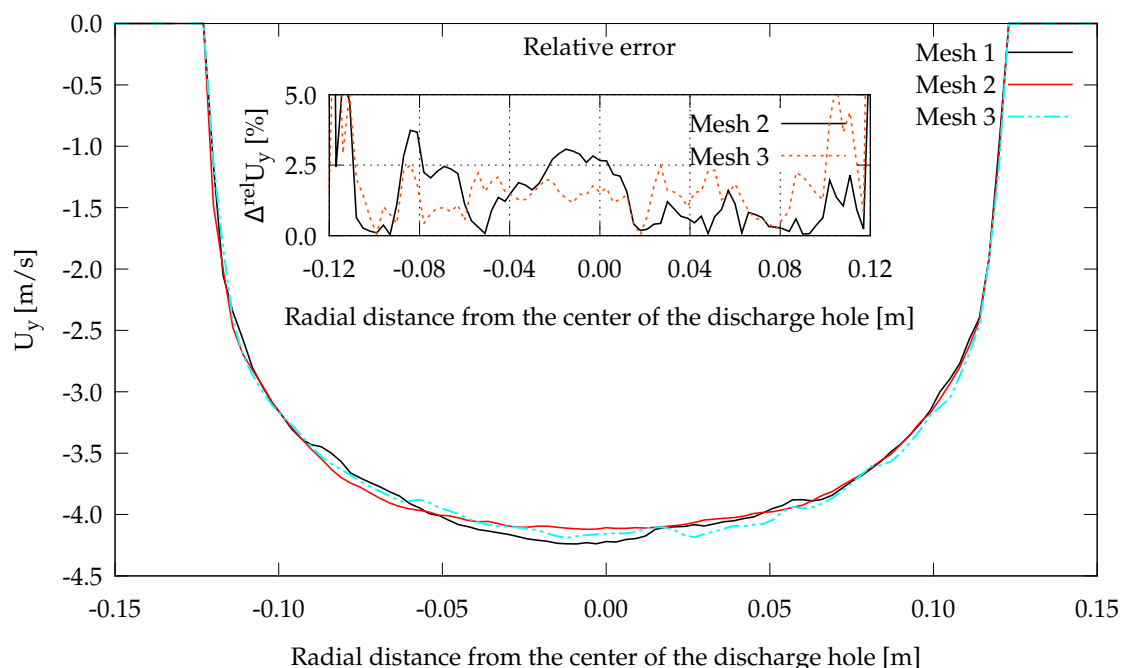


Figure 5: Velocity profile in the  $y$  direction along the diameter of the discharge hole for  $t = 0.4s$ . (Inset) Relative error on velocity for the solutions obtained with meshes (2) and (3).

In order to obtain the remaining liquid height inside the tank, Figure (6) shows a sequence of the discharge procedure during the first 15 seconds of the evolution. In particular we show a case with a non-centered hole which center is located in  $(0.4; 0.0; 0.4)m$ . The total pressure field and the velocity field are shown in each cut of the geometric domain. It can be seen that the initial total pressure at the bottom equals the liquid column and the maximum Reynolds number at the discharge hole is nearly  $Re_D = 10^6$  from the very beginning of the transient and during the first five seconds of the dynamics.

Due to the fact that in the present problem the relevant variable to describe the behavior is the remaining liquid height, in Figure (7) we show in a comparative manner the computed liquid height. In particular, the remaining liquid height in the tridimensional calculations was determined in two ways:

- Method 1: By a local measurement over a vertical line of the level of the indicator function for different values:  $\alpha = 0.01$ ,  $\alpha = 0.50$  and  $\alpha = 0.99$ .
- Method 2: By measuring the volumetric flow in the physical group *Hole* and applying the mass conservation.

In particular, we display the associated curves with the case shown in Figure (6), with a non-centered hole, and an identical case but with a centered discharged hole. It can be seen that almost no difference exists between them. As a lower threshold for the discharge time, we also display the theoretical solution given by Eq.(2). It can be seen that the numerical solutions and the theoretical solution have a similar behavior but the last one predicts a quicker discharge time. The difference could be due to the fact that the theoretical solution does not take into account the sudden contraction that occurs near the hole neither consider the dissipation caused by the turbulent flow.

We also display the computed liquid height obtained in a local manner (*method 1*) for three different values of the indicator function. The gradient of the indicator function widespread in approximately 6 cm in the vertical direction. As a check of consistency, from Figure (7) it can be seen that the evolution obtained with *method 2* lies right in the middle of the evolutions computed by *method 1*. This points out that the numerical schemes selected transport the indicator function  $\alpha$  in an accurate manner without loss of mass.

Time [s]	$ U _{mesh\ 3}^{hole} [\frac{m}{s}]$	$ U _{mesh\ 2}^{hole} [\frac{m}{s}]$	$ U _{mesh\ 1}^{hole} [\frac{m}{s}]$
0.0	0.00000	0.00000	0.00000
0.2	3.32454	3.37809	3.37829
0.4	3.31183	3.36176	3.36162
0.6	3.29691	3.34673	3.34545
0.8	3.28203	3.33141	3.32985
1.0	3.26707	3.31511	3.31382

Table 4: Modulus of velocity averaged in the discharge hole area.

Time [s]	$\Delta U _{mesh\ 2}^{hole} [\%]$	$\Delta U _{mesh\ 3}^{hole} [\%]$
0.0	0.000	0.000
0.2	0.006	1.591
0.4	0.004	1.481
0.6	0.040	1.451
0.8	0.050	1.436
1.0	0.040	1.411

Table 5: Relative error of the modulus of velocity averaged in the discharge hole area.

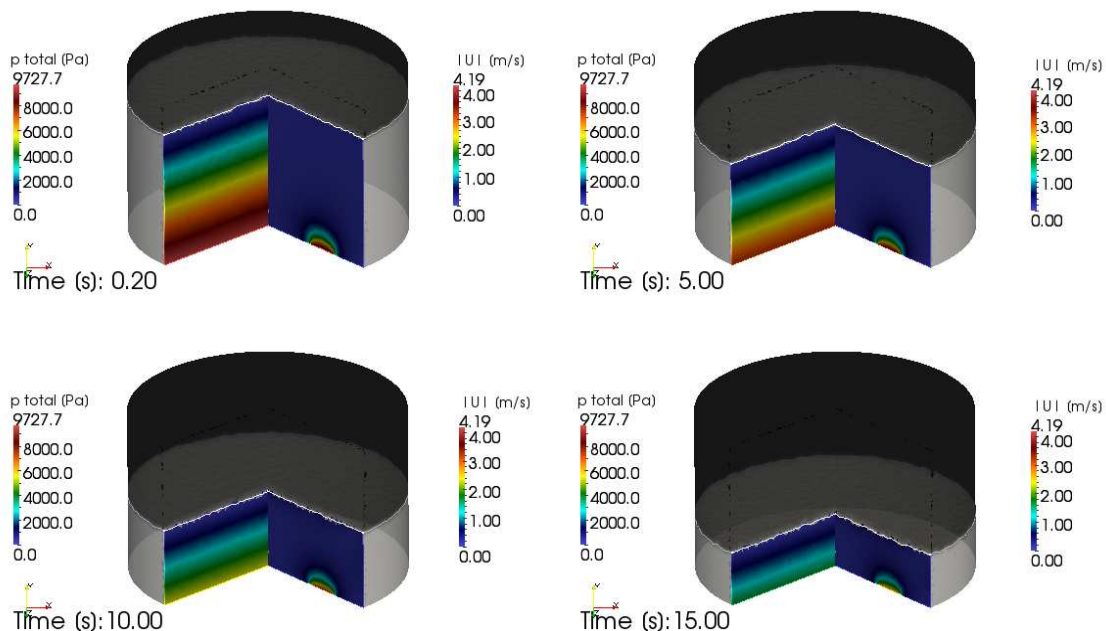


Figure 6: Simple model of a draining tank full of light water up to a height of  $1m$ . The radius of the tank is  $1m$  and a non-centered discharge circular area of  $0.24m$  of diameter is located at the bottom of it. In the left cut we show the total pressure field, while in the right side of the cut we show the modulus of the velocity during a time sequence of the draining process. The remaining liquid height after 15 seconds of evolution is  $0.4m$ .

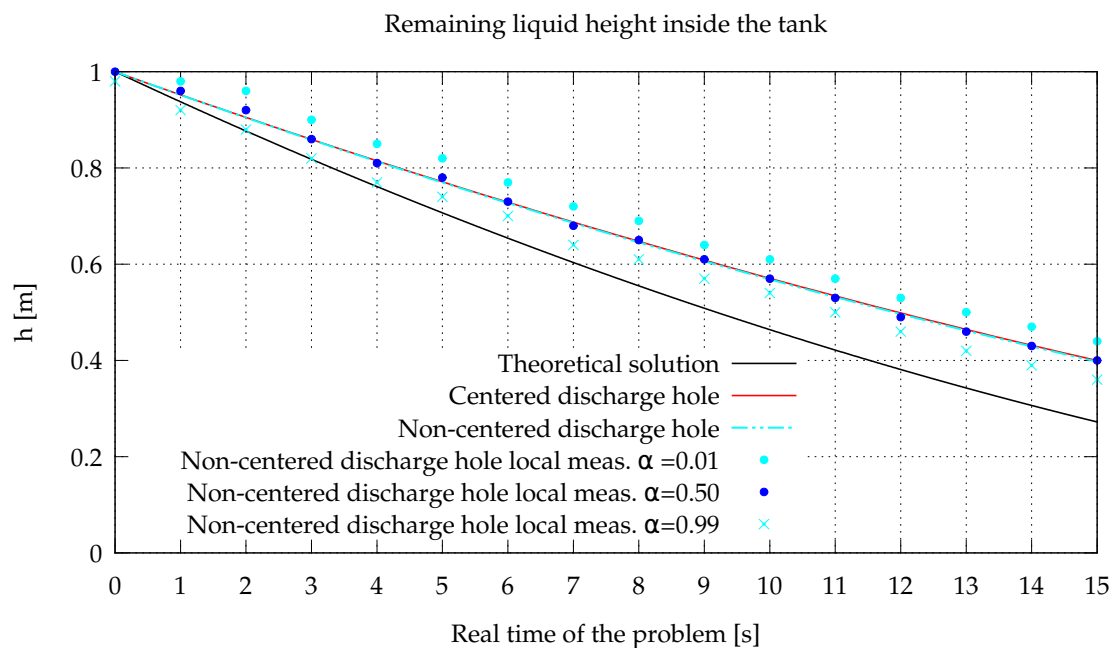


Figure 7: Temporal evolution of the remaining liquid height inside the tank. Three cases were considered: (A) The theoretical approximation. (B) Simple model with OF with a centered discharge hole. (C) Simple model with OF with a non-centered discharge hole. No remarkable difference is observed on the global discharge dynamics between the cases with a centered hole and non-centered hole. The location of the interphase obtained by a local measurement of the indicator function ( $\alpha$ ) for different values (*method (1)*), contains right in the middle the results obtained by *method (2)*.

## 6 CONCLUSIONS

In this work we have shown a numerical model to analyze the main features of the discharge dynamics of a cylindrical tank using the OpenFOAM framework.

We have shown a possible and accurate chain of tools that allow us to successfully made simulations to evaluate the performance of the system during the required time of the problem.

The three grid analysis allowed us to quantify the uncertainty introduced by the space discretization in compromise with the execution times. For the ranges and meshes analyzed, the relative error is lower than  $<1\%$  for the modulus of velocity averaged in the discharge hole area, while the relative error of the velocity profile in the discharge hole is lower than  $<5\%$  far away from edges.

By computing the position of the free surface with two different methods, we verify that the indicator function is transported in an accurate manner without a significant mass loss. We also evaluate that the position of the discharge orifice at the bottom of the tank does not play any significant role on the global draining dynamics.

This simple problem allow us to setup all the details involved in a high quality CFD analysis according to our computing capacity due to the perspective of this work implies a more complex and detailed geometry.

## ACKNOWLEDGMENTS

LMR was financed by CNEA. LMR acknowledges Ezequiel Fogliato and Jorge Salinas for fruitful discussions.

## REFERENCES

- Bird R., Stewart W., and Lightfoot E. "Transport Phenomena", volume 2nd Edition. John Wiley & Sons, 2002.
- Dari E. and Buscaglia G. "Mesh optimization: how to obtain good unstructured 3D finite element meshes with not-so-good mesh generators". *Structural Optimization*, 8:181–188, 1994.
- Durbin P. and Pettersson-Reif B. "Statistical Theory and Modeling for Turbulent Flows", volume 2nd Edition. Wiley, 2011.
- EPRI. "High - performance computing in the electric power industry.". *EPRI TECHNOLOGY INSIGHTS*, 2014.
- Ferziger J. and Perić M. "Computational methods for fluid dynamics", volume 3rd Edition. Springer, 2002.
- Geuzaine C., Marchandise E., and Remacle J. "An Introduction to Geometrical Modelling and Mesh Generation". 2009a.
- Geuzaine C., Marchandise E., and Remacle J. "Gmsh: a three-dimensional finite element mesh generator with built-in pre- and post-processing facilities". *Int. J. Num. Meth. Eng.*, 79:1309–1331, 2009b.
- Hilal R. "Deterministic safety analysis of research reactors.". ME thesis, Instituto Balseiro. UNCu, 2012.
- Hirt C. and Nichols B. "Volume of Fluid (VOF) Method for the Dynamics of Free Boundaries". *J. Comp. Phys.*, 39:201–225, 1981.
- IAEA-TECDOC-1379. "Use of computational fluid dynamics codes for safety analysis of nuclear reactor systems. 2003.
- Jasak H. "Error Analysis and Estimation for the Finite Volume Method with Applications to Fluid Flows". Ph.D. thesis, Imperial College, 1996.
- NEA. "Best practice guidelines for the use of CFD in nuclear reactor safety applications.". Nuclear Energy Agency, 2007.
- OpenFOAM®. "http://www.openfoam.com/". 2014.
- Pellegrini F. "Contributions au partitionnement de graphes parallèle multi-niveaux". Ph.D. thesis, Université de Bordeaux I, 2009.
- SG.OpenFoam.ESI. "C++ Source Guide", volume Version 2.2.1. 2013.
- UG.OpenFoam.ESI. "User Guide", volume Version 2.2.1. 2013.